Neimark Sacker bifurcations and non-linear energy exchange in chains of non-linear oscillators

Gabriel Hurel, Sébastien Baguet, Claude-Henri Lamarque

Author manuscript, published in "International Journal of Non-Linear Mechanics", 104057 (2022)
DOI: 10.1016/j.ijnonlinmec.2022.104057
The final publication is available at Elsevier via www.sciencedirect.com

Neimark Sacker bifurcations and non-linear energy exchange in chains of non-linear oscillators

Gabriel HUREL[a,b,*], Sbastien BAGUET[b], Claude-Henri LAMARQUE[a]

[a] *Univ Lyon, ENTPE, CNRS UMR5513, LTDS, F-69518, France*
[b] *Univ Lyon, INSA-Lyon, CNRS UMR5259, LaMCoS, F-69621, France*

Abstract

We treat a chain of oscillators with linear stiffness and internal and external cubic non-linearities. The method of harmonic balance is used to determine the non-linear modes of the Hamiltonian system. For each equilibrium point, a stability analysis is performed by means of the associated monodromy matrix. The numerical results shows that branch points, limit points and Neimark-Sacker bifurcations exist in the system. The aim of the paper is to study how they drive the energy in the system: branch points make energy transfer between non-linear modes possible, while Neimark-Sacker bifurcations can lead to chaotic behaviour. As the number of oscillators increases, the energy required to reach the first Neimark-Sacker bifurcation follows a remarkable regularity.

Keywords: Non-linear chain, non-linear mode, Bifurcation, Harmonic balance method, Vibration control

1. Introduction

The literature on non-linear chains of oscillators comprises numerous contributions [1, 2]. Indeed, atypical and interesting phenomena exist in such systems. For example, a wave can propagate in a non-linear medium without scattering, which means that the energy can be localized [3, 4, 5]. Such a phenomenon is called a soliton in the case of a propagating wave and of a breather for a stationary wave [6, 7]. Therefore, nonlinear chains appear as promising candidates on which to build a vibratory or acoustic control [8, 9]. The vibratory energy can be localized in order to be dissipated or on the contrary scattered to be transferred to another frequency domain.

In order to study such chains, several method exist: analytical methods, numerical methods or semi-anaytical methods. Flach et al. [10] studied the energy threshold of the FPU problem with qualitative analyses based on the normal form method. Verhulst [11] and Andrianov et al. [12] identified mode coupling and interactions between high and low frequencies. The chain can be modelled as a discrete system with point masses or as a continuous material if it is long enough. The transition from a discrete to a continuous system can be considered to simplify the modelling [13].

In this paper, a chain with a large number of oscillators is considered. A semi-analytical method and a bifurcation analysis are used to predict and explain its dynamic behaviour. Bifurcations not only permit monitoring changes in the global dynamics of the system when its parameters are varied. [14, 15, 16, 17] but also control the exchange of energy between the different non-linear modes. In order to clearly explain our approach, a system with few degrees of freedom will first be considered. Then, the proposed method will be applied to a larger system. In the next section, we describe the system and its linearisation. In Section 3 we first consider a chain with a few oscillators. We use the harmonic balance method to compute the non-linear modes and the bifurcations. We compare the results with direct time integration. In Section 4 we study the bifurcations of the system with a large number of masses. Finally, conclusions are drawn in Section 5.

*Corresponding author
Email addresses: gabriel.hurel@entpe.fr (Gabriel HUREL), sebastien.baguet@insa-lyon.fr (Sbastien BAGUET), claude-henri.lamarque@entpe.fr (Claude-Henri LAMARQUE)

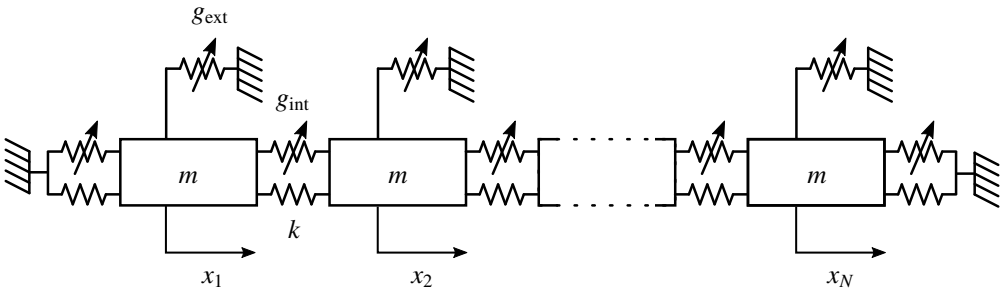

Figure 1: Chain of N non-linear oscillators.

2. System

We consider a chain of N masses m linked with $N+1$ linear springs with stiffness k as shown in Fig. 1 Both ends of the chain are grounded. The non-linearity is introduced in two different ways:

- internal non-linearity: between two consecutive masses.
- external non-linearity: between each mass and the ground

A damping coefficient c is introduced. The dynamics of the system can be described by N equations:

$$m\ddot{x}_n + c\dot{x}_n + k(-x_{n-1} + 2x_n - x_{n+1}) + g_{\text{int}}(x_n - x_{n-1}) + g_{\text{int}}(x_n - x_{n+1}) + g_{\text{ext}}(x_n) = f_n \sin(\omega t + \theta),\ 1 \leq n \leq N \quad (1)$$

where x_n is the horizontal displacement of the mass n (we consider $x_0 = x_{N+1} = 0$), f_n, ω and θ are the amplitude, the frequency and the phase of the external forcing respectively and g_{int} and g_{ext} are nonlinear functions. In our study, both non-linearities are purely cubic:

$$g_{\text{int}}(x) = k_{\text{int}}x^3 \quad (2)$$

$$g_{\text{ext}}(x) = k_{\text{ext}}x^3 \quad (3)$$

where k_{int} and k_{ext} are constant coefficients. The system equations can be written in matrix form:

$$\mathbf{M}\ddot{X}(t) + \mathbf{C}\dot{X}(t) + \mathbf{K}X(t) + G((X(t)) = F(t) \quad (4)$$

where $X(t)$, $\mathbf{M}$, $\mathbf{K}$, $G(X)$ and $F(t)$ are the displacement vector, mass matrix, linear stiffness matrix, non-linear forces vector and external force vector, respectively. The mass matrix is a diagonal matrix $\mathbf{M} = m\mathbf{I}$ where $\mathbf{I}$ is the unity matrix. The linear stiffness matrix is a tridiagonal matrix:

$$\mathbf{K} = k\begin{pmatrix} 2 & -1 & 0 & \cdots & 0 \\ -1 & 2 & -1 & \ddots & \vdots \\ 0 & \ddots & \ddots & \ddots & 0 \\ \vdots & \ddots & -1 & 2 & -1 \\ 0 & \cdots & 0 & -1 & 2 \end{pmatrix} \quad (5)$$

If we consider the linearised undamped system ($k_{\text{int}} = k_{\text{ext}} = c = 0$), we can calculate the linear undamped eigenmodes ϕ_p and write X as:

$$X = \mathbf{\Phi}Q \quad (6)$$

where $\mathbf{\Phi} = (\phi_1, \ldots, \phi_N)$ is the matrix of the normal modes and $Q = (q_1^T, \ldots, q_N^T)^T is$ the vector of generalized displacement. The frequency of mode p is given by:

$$\omega_p = 2\omega_0 \sin\left(\frac{p\pi}{2N+2}\right) \quad (7)$$

where $\omega_0 = \sqrt{\frac{k}{m}}$. The matrix equation of the system with generalized coordinates read:

$$\mathbf{I}\ddot{Q} + \frac{c}{m}\mathbf{I}\dot{Q} + \mathbf{\Omega}^2 Q + \mathbf{\Phi}^\intercal G(\mathbf{\Phi}Q) = \mathbf{\Phi}^\intercal F \tag{8}$$

where

$$\mathbf{\Omega} = \mathrm{diag}(\omega_1, \omega_2, \cdots, \omega_N) \tag{9}$$

or

$$\frac{\mathrm{d}^2 q_n}{\mathrm{d}\tau^2} + \lambda \frac{\mathrm{d}q_n}{\mathrm{d}\tau} + r_n^2 q_n + g_n(q_1, \cdots, q_N) = f_{qn},\ 1 \leq n \leq N \tag{10}$$

with the dimensionless time $\tau = \omega_1 t$, $\lambda = \frac{c}{m}$, $r_n = \frac{\omega_n}{\omega_1}$ and g_n the modal non-linear forces on mode n:

$$g_n(q_1, \cdots, q_N) = \sum_{i,j,k \in [1,N]} a_{ijk}\, q_i q_j q_k \tag{11}$$

The ratios r_n are given in Fig. 2 for several values of N. For high values of N, the ratio r_n is close to n for the first eigenmodes:

$$r_n = \frac{\omega_n}{\omega_1} = \frac{\sin\left(\frac{n\pi}{2N+2}\right)}{\sin\left(\frac{\pi}{2N+2}\right)} = n + n\left(1 - n^2\right) O\left(\frac{1}{N}\right) \tag{12}$$

For $N = 25$, the frequency ratios of the first five eigenmodes are very close to integers (and internal resonances are expected).

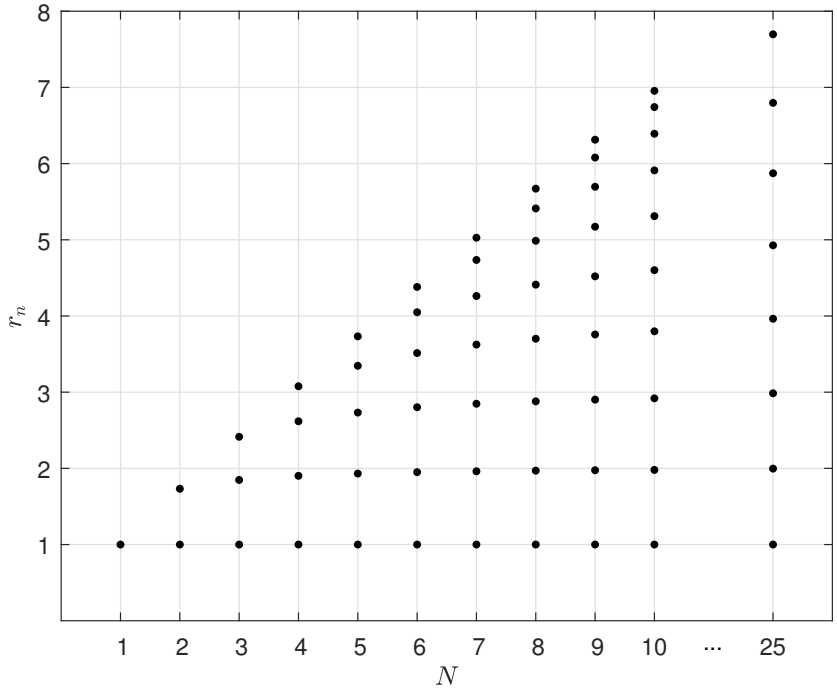

Figure 2: Frequency ratios $r_n = \frac{\omega_n}{\omega_1}$ of the system for several values of N.

3. Analysis of the system for $N = 3$

Firstly, in this section, we consider a chain with only three masses. The objective is to determine what phenomena are present that can drive the energy distribution in the chain. For this, a modal approach seems relevant. In this section, for all figures we take the following parameters:

$$m = 1,\ k = 1,\ k_{\text{int}} = 0,\ k_{\text{ext}} = 1 \tag{13}$$

3.1. Harmonic balance method

To analyze this non-linear system, the harmonic balance method (HBM) is used. The response of the system is assumed to be a periodic function and can therefore be expressed as a truncated Fourier series:

$$q_n(t) = c_n + \sum_{h=1}^{H} a_{nh}\cos(\omega h t) + b_{nh}\sin(\omega h t) \tag{14}$$

where H is the number of harmonics retained in the response. Replacing the Eq. (14) in Eqs. (10), yields a system of N equations with $N(2H + 1)$ unknowns. To find solutions of this system, we use the ManLab software package [18] which relies on the asymptotic numerical method (ANM). . In order to use the ANM, a quadratic recast of the equations is mandatory. To this end, additional variables are introduced and the cubic terms are written as:

$$u_n^3 = u_n v_n \tag{15}$$

where $v_n = u_n^2$. If a solution for a given value of a system parameter is known, the solution for a closed value can be found by continuation technique.

3.2. Hamiltonian system

Now we consider the system with no damping ($\lambda = 0$) and no forcing ($f_{qn} = 0$).

$$\frac{\mathrm{d}^2 q_n}{\mathrm{d}\tau^2} + r_n^2 q_n + g_n(q_1, \cdots, q_N) = 0,\ n \in [1, N] \tag{16}$$

The linear modes ϕ_n are solution of this Hamiltonian non-linear system for very low amplitude. Therefore, they are used as initial solutions for the computation of the non-linear modes. The non-linear modes are calculated as periodic solutions of (16) by increasing the amplitude with continuation. In Fig. 3 the non-linear normal modes of the system are presented for $N = 3$. They are interesting because they represent the skeleton curves of the response of the system.

Their L^2 norm is given by:

$$|q_n|_{L^2} = \sqrt{c_n^2 + \frac{1}{2}\sum_{h=1}^{H}(a_{hn}^2 + b_{hn}^2)} \tag{17}$$

Its projections on the linear modes q_i are plotted in Fig. 3a. For each non-linear mode, the contribution of several linear modes can be observed. For instance, q_1 and q_3 participate in the non-linear modes 1 and 3, whereas only q_2 contributes to the non-linear mode 2. This can be explained by the symmetry of the shape of the linear and non-linear modes: the modes 1 and 3 are symmetric whereas the mode 2 is antisymmetric as shown in the next Section.

The contribution of significant harmonics is given in figures 3b, 3c and 3d.

Now we evaluate the accuracy of the solution. Since no energy is exchanged with the external systems, the Hamiltonian $\mathcal{H}$ of the system is constant:

$$\mathcal{H} = \mathcal{K} + \mathcal{U} + \mathcal{S} \tag{18}$$

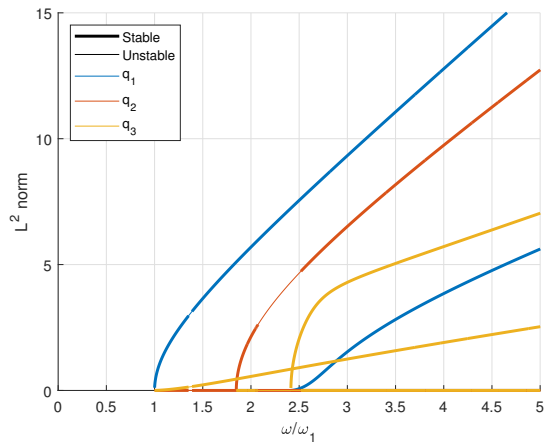

(a) Hamiltonian system

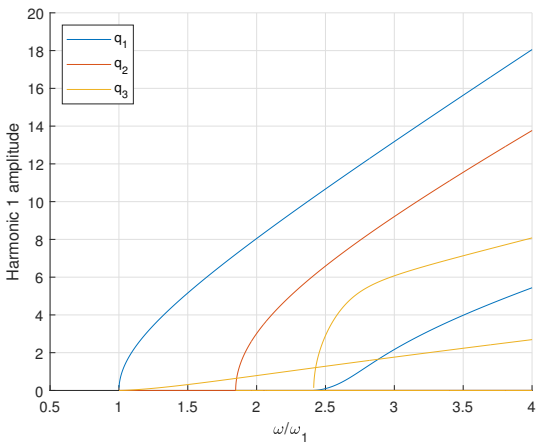

(b) Amplitude of harmonic 1

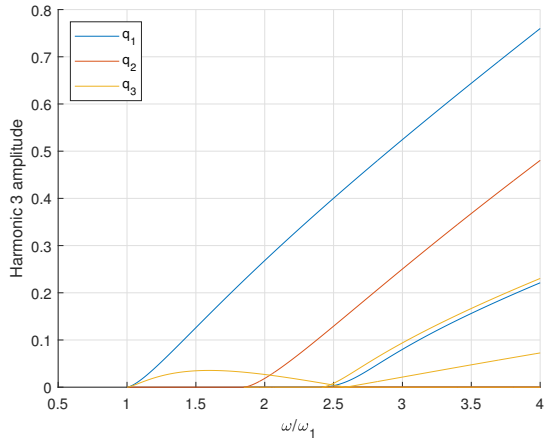

(c) Amplitude of harmonic 3

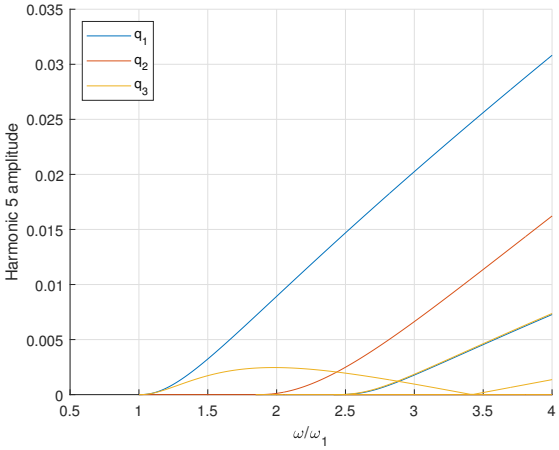

(d) Amplitude of harmonic 5

Figure 3: Non-linear normal modes and significant harmonics (1, 3 and 5) with $H = 20$.

where $\mathcal{K}$ is the kinetic energy, $\mathcal{U}$ the linear potential energy and $\mathcal{S}$ the potential energy of non-linear terms:

$$\mathcal{K} = \sum_{n=1}^{N} \frac{m}{2} x_n^2 \tag{19}$$

$$\mathcal{U} = \sum_{n=1}^{N-1} \frac{k}{2} (x_{n+1} - x_n)^2 + \frac{k}{2} \left(x_1^2 + x_N^2 \right) \tag{20}$$

$$\mathcal{S} = \sum_{n=1}^{N-1} \frac{k_{\text{int}}}{4} (x_{n+1} - x_n)^4 + \frac{k_{\text{int}}}{4} \left(x_1^4 + x_N^4 \right) + \sum_{n=1}^{N} \frac{k_{\text{ext}}}{4} x_n^4 \tag{21}$$

Their time evolution are plotted in Fig. 4a over one period for $N = 3$ and $H = 3$. The rate of variation of $\mathcal{H}$ indicates if the solution is acceptable or if we need to consider more harmonics, i.e., to increase H. We define the relative error E_r on the energy as :

$$E_r = \frac{\max(\mathcal{H}) - \min(\mathcal{H})}{\frac{1}{T} \int_0^T \mathcal{H}(t) \mathrm{d}t} \tag{22}$$

where $T = \dfrac{2\pi}{\omega}$ is the period. The Fig. 4b shows that the relative error E_r decreases as the number of harmonics H in the solution increases. For $H = 20$, the relative error is less than 1×10^{-12}. We consider this error acceptable and choose $H = 20$ for $N = 3$.

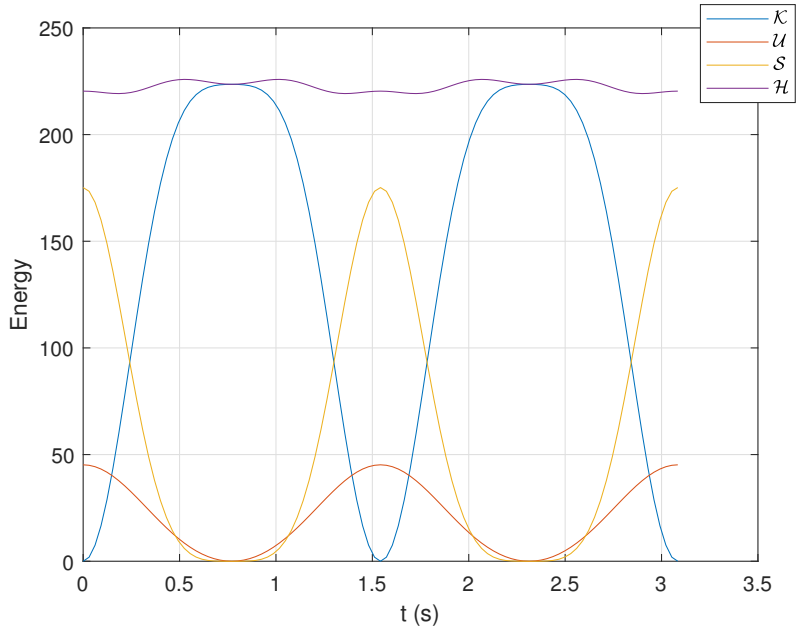

(a) $\omega = 2\omega_1$

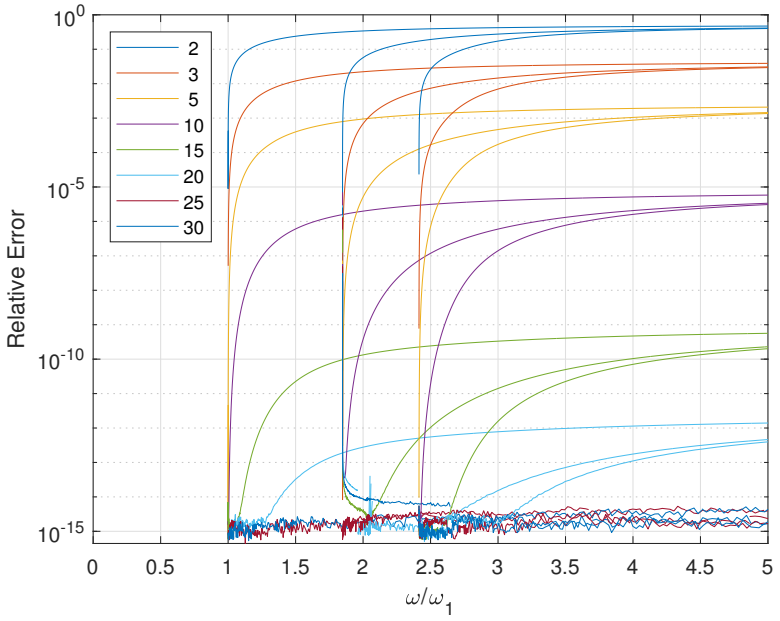

(b) E_r

Figure 4: Energy over one period for $H = 3$ (a) and relative error E_r for several values of H for $N = 3$ (b).

3.3. Shapes of solutions

It is interesting to follow a non-linear mode to see how its shape evolves with amplitude. In Fig. 5, the shapes of the modes are shown for very low amplitude corresponding to linear modes and for high amplitude. We recall that the linear mode p can be expressed with sine functions:

$$x_i = \sin\left(\frac{ip\pi}{N+1}\right) \tag{23}$$

The symmetry of the linear modes is preserved for non-linear modes. The shape of mode 2 does not change. Indeed, only the linear mode 2 participates in the non-linear mode 2. For very high amplitude, the displacements of a mass can take only three values: $x_i \in \{-1, 0, 1\}$. Interestingly, for the non-linear mode 3, the energy is localized only on the second mass.

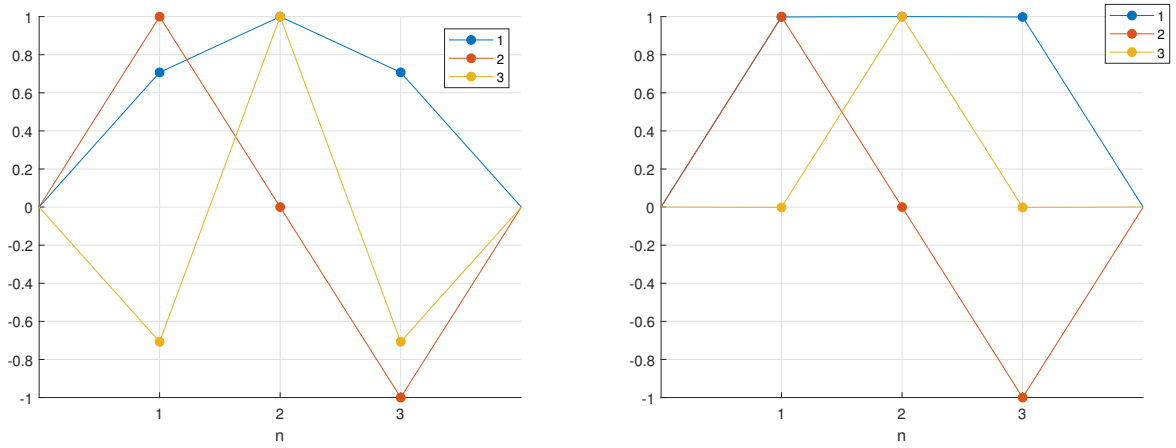

(a) Low amplitude (linear)

(b) High amplitude

Figure 5: Shape of the non-linear modes normalized with maximum value for very low amplitude and very high amplitude on each branches for $N = 3$.

For $N = 3$, the equations of the system read:

$$m\ddot{x}_1 + k(2x_1 - x_2) + k_{\text{ext}}x_1^3 = 0 \tag{24}$$
$$m\ddot{x}_2 + k(2x_2 - x_1 - x_3) + k_{\text{ext}}x_2^3 = 0 \tag{25}$$
$$m\ddot{x}_3 + k(2x_3 - x_2) + k_{\text{ext}}x_3^3 = 0 \tag{26}$$

When $x \longrightarrow \infty$, the linear part can be neglected:

$$m\ddot{x}_1 + k_{\text{ext}}x_1^3 = 0 \tag{27}$$
$$m\ddot{x}_2 + k_{\text{ext}}x_2^3 = 0 \tag{28}$$
$$m\ddot{x}_3 + k_{\text{ext}}x_3^3 = 0 \tag{29}$$

We note that when the amplitude of the displacements increase, the equations of the system tend to be decoupled. This explain the localization of the energy in the nonlinear modes.

3.4. Stability of the solutions

In order to predict the behaviour of the system, it is necessary to find the stability of each solution. To do this, we use the Newmark-beta time-integration method with $\gamma = \frac{1}{2}$ and $\beta = \frac{1}{4}$ to calculate the Monodromy matrix from which

the Floquet multipliers μ_i are obtained [19, 20]. The solution is stable if all if all Floquet multipliers μ_i are such that $|\mu_i| \leq 1, \forall i$, and unstable otherwise. Figure 6 shows the evolution of the Floquet multipliers for the non-linear modes 1 and 2 in the complex plane and their modulus. A unstable zone exists for $1.356 < \frac{\omega}{\omega_1} < 1.386$ for the non-linear mode 1 and for $2.07 < \frac{\omega}{\omega_1} < 2.51$ for the non-linear mode 2.

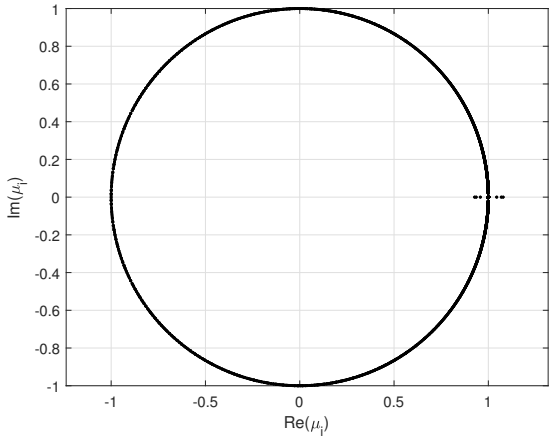

(a) Floquet multipliers in complex plane for the first non-linear mode.

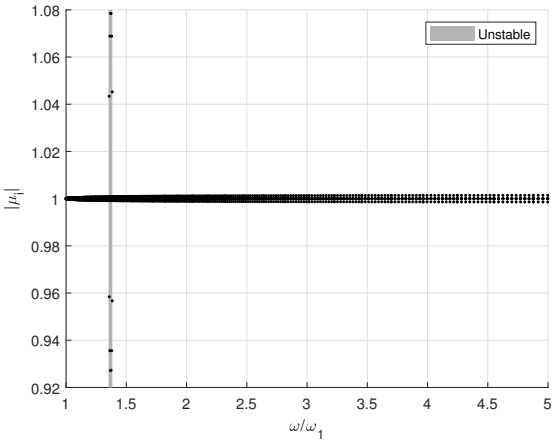

(b) Norm of Floquet multipliers for the first non-linear mode.

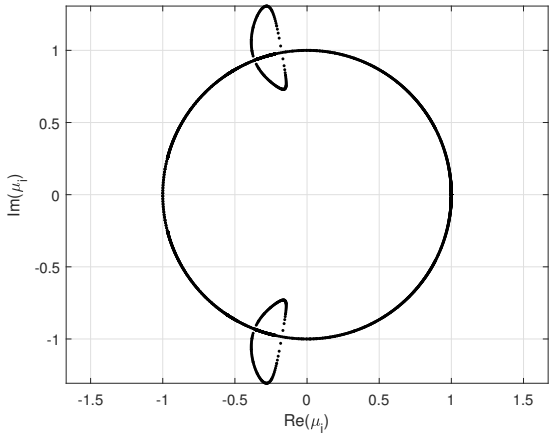

(c) Floquet multipliers in complex plane for the second non-linear mode.

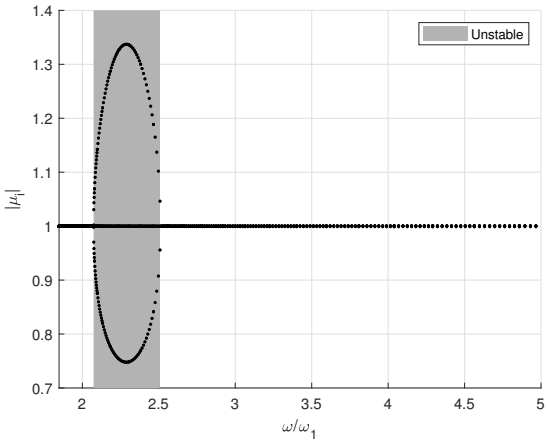

(d) Norm of Floquet multipliers for the second non-linear mode.

Figure 6: Floquet multipliers of the first two non-linear modes in the complex plane and their norm. Unstable zones appear in grey.

3.5. Forced system

Here, we consider the system (10) with damping λ and excited by modal forces f_{qn}. Fig. 7 gives the response of the system for different cases of force. We trace the L^2 norm of the Fourier coefficients of each generalized coordinate q_i over frequency. It can be verified that the non-linear modes (dashed lines) computed in the previous section serve as backbone curves for the response curves.

If only one mode is excited, the response curves are relatively simple but they become more complex when several modes are excited due to non-linear interactions. We remark in Fig. 7d that the peaks of modes 1 and 2 are not on the

skeleton curves. This difference comes from the coupling with other modes. For instance, at the peak of the response curve of non-linear mode 1, a fraction of the energy is located on mode 2.

The stability of the non-linear modes gives a good idea of the stability of the response curve. As classically observed in the case of non-linear resonance, the part of the response curve below the folded peak in Figs. 7a, 7b and 7c is unstable. In Figs. 7b and 7d, the unstable zone of the non-linear mode 2 for $2.07 < \frac{\omega}{\omega_1} < 2.51$ also exist in the response of the system. However, in Fig 7a, the unstable zone of the non-linear mode 1 near $\frac{\omega}{\omega_1} = 1.4$ does not does not appear in the response. This can be explained by the damping existing in the forced system. In addition, the unstable zones of the response curves in Fig. 7d are much more complex and cannot be simply inferred from the stability of the non-linear modes.

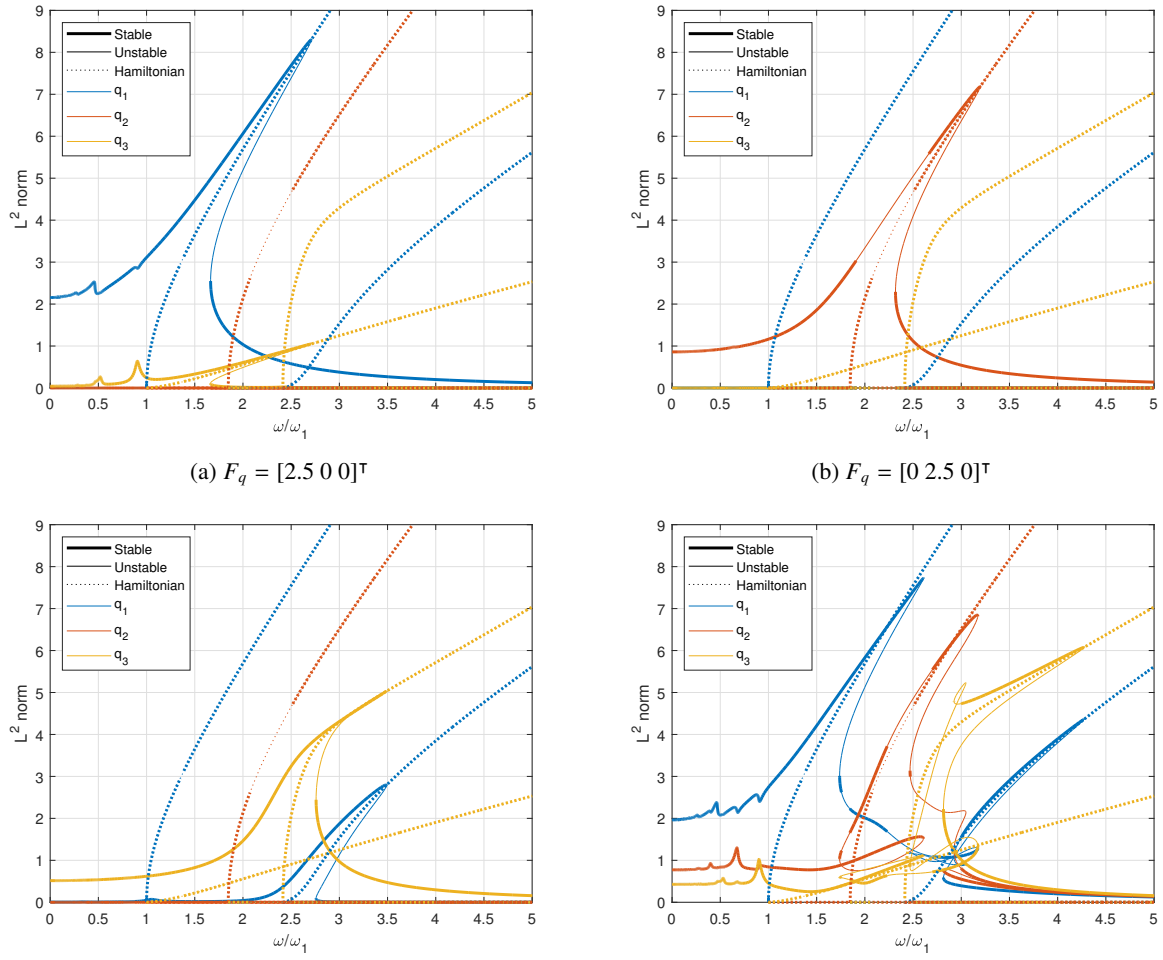

(a) $F_q = [2.5\ 0\ 0]^\intercal$

(b) $F_q = [0\ 2.5\ 0]^\intercal$

(c) $F_q = [0\ 0\ 2.5]^\intercal$

(d) $F_q = [2.5\ 2.5\ 2.5]^\intercal$

Figure 7: Response of the system ($N = 3$) with $\lambda = 0.01$ and an excitation on each eigenmode computed with HBM ($H = 20$).

3.6. Bifurcation analysis

A bifurcation is present when the modulus of a Floquet multiplier μ_b becomes higher than one. Its nature can be determined with the value of the Floquet multiplier [16]:

- $\mathrm{Im}(\mu_b) = 0$ and $\mathrm{Re}(\mu_b) \geq 1$: the bifurcation is a branch point or a limit point ;

- $\mathrm{Im}(\mu_b) \neq 0$: the bifurcation is a Neimark-Sacker bifurcation ;
- $\mathrm{Im}(\mu_b) = 0$ and $\mathrm{Re}(\mu_b) \leq 1$: the bifurcation is a doubling period bifurcation.

Figure 6 shows the Floquet multipliers of the first two non-linear modes in the complex plane and their modulus. For the first non-linear mode, the Floquet multipliers cross the unit circle through the real axis, which leads to two branch points.

For the second mode, tthe Floquet multipliers cross the unit circle with a non-zero imaginary part, which leads to two Neimark-Sacker bifurcations. Two Neimark-Sacker bifurcation exists.

Fig. 8 shows so-called frequency-energy plots, i.e. energy $\mathcal{H}$ versus frequency, together with bifurcations and stability for two cases:

- $k_{\text{ext}} = 0$, $k_{\text{int}} = 0.1$
- $k_{\text{ext}} = 0.1$, $k_{\text{int}} = 0$

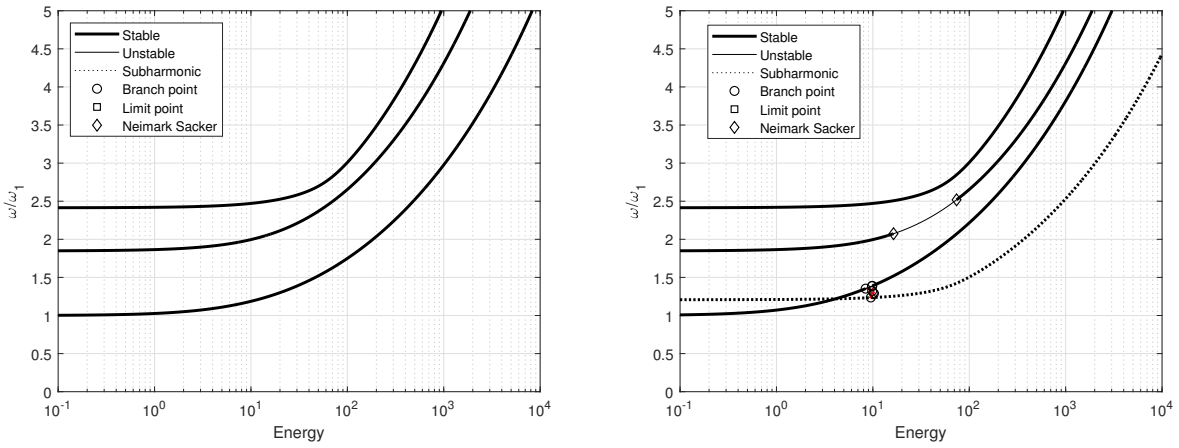

(a) $k_{\text{ext}} = 0$, $k_{\text{int}} = 0.1$ (b) $k_{\text{ext}} = 0.1$, $k_{\text{int}} = 0$

Figure 8: Frequency-energy plot for $N = 3$.

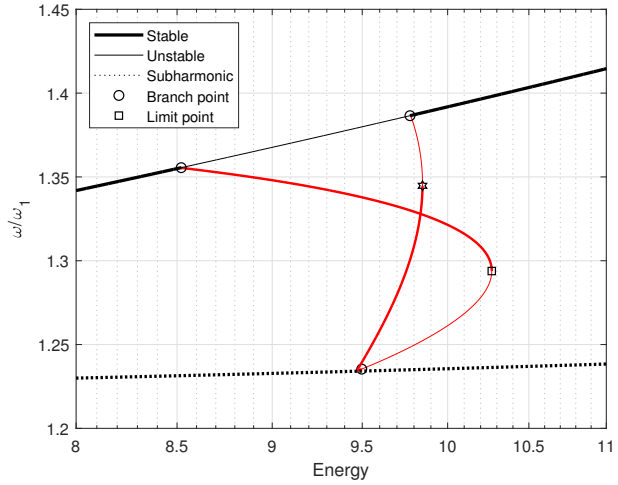

Figure 9: Zoom of Fig. 8b. Secondary branch between non-linear mode 1 and subharmonic of the non-linear mode 3.

It can be noticed that no bifurcations are present in the case with only local non-linearity k_{int} (Fig8a). The type of non-linearity has a great impact on the presence of bifurcations.

In the other case (Fig8b, two types of bifurcations exist, branch point and Neimark-Sacker bifurcations. These bifurcations are interesting because they are responsible for energy exchanges between modes. In order to better understand how these exchanges occur, we will analyse each type of bifurcation in more detail.

3.6.1. Branch point

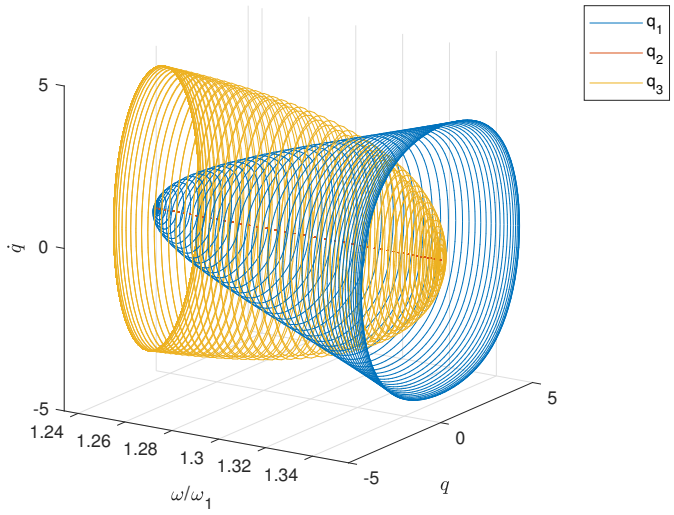

Figure 10: Phase diagram along the secondary branch between non-linear modes 1 and 3.

In Fig. 8a, several branch points are present on non-linear mode 1. From these points, additional branches connect non-linear mode 1 to the subharmonic of non-linear mode 3 as shown in Fig. 9. A limit point splits each secondary branch in a stable zone and an unstable zone. Similar phenomenon has been studied by Volvert et. al [21].

Fig. 10 gives the phase portrait while following the secondary branches. An evolution from mode 1 to mode 3 can be observed. Mode 2 is represented by a straight line with null amplitude because it is not involved in this branch due to the symmetry of the shape. This bifurcation permits an energy transfer from a mode to another one because at this level of energy, the natural frequency of the non-linear mode 1 ω_1 is close to one half of the natural frequency of the non-linear mode 3 ω_3:

$$\omega_1 \approx \frac{\omega_3}{2} \tag{30}$$

Time responses of the Hamiltonian system initialized with solutions on mode 1 branch (see Fig. 9) for four different energy levels are plotted in Fig. 11 with several initial energies on the mode 1. According to Fig. 9, the initial solution corresponding to an energy level $E = 8.5$ is located in the stable zone of mode 1 but is very close to the branch point. The three other initial conditions $E = 9, 9.5, 9.7$ are located in the unstable zone between the two branch points. It can be observed that, when the initial solution is unstable, the amplitude of mode 3 increases and the system oscillates in a quasi-periodic regime.

The Poincaré section defined by $q_1 = 0$ and $\dot{q}_1 > 0$ corresponding to Fig. 11d is plotted in Fig. 12. The closed loop obtained for q_3 confirms the quasiperiodicity of the motion.

This type of energy exchange is interesting because it takes place between only two modes. Energy can be transferred in a controlled way. However, as shown in Fig. 7a, this exchange may not take place if the damping is too large.

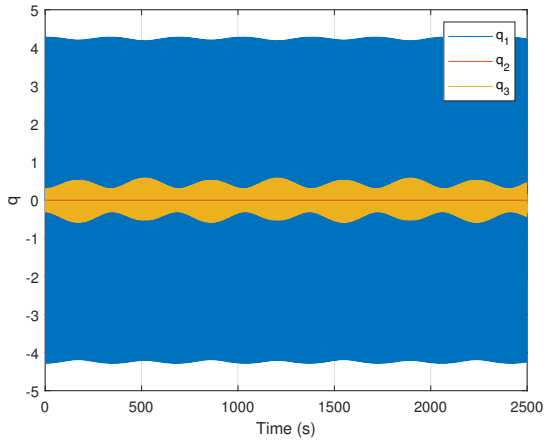

(a) $E = 8.5$

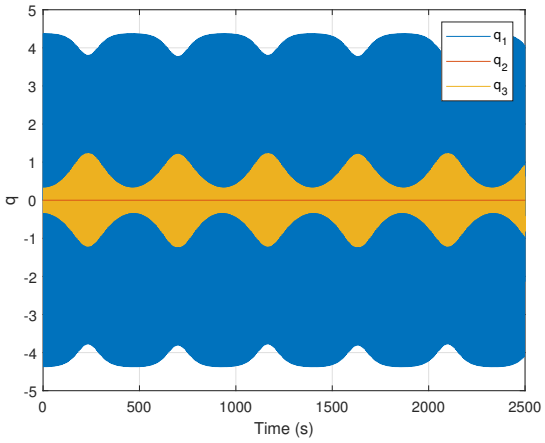

(b) $E = 9$

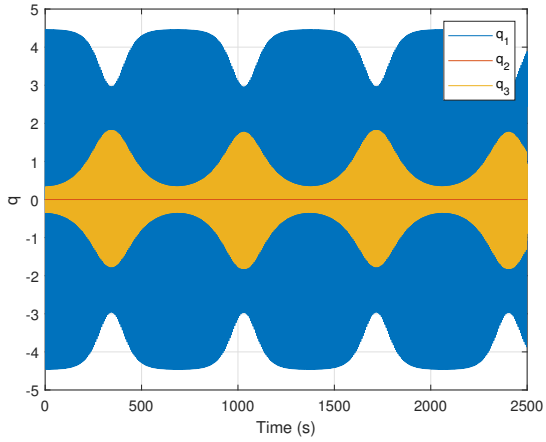

(c) $E = 9.5$

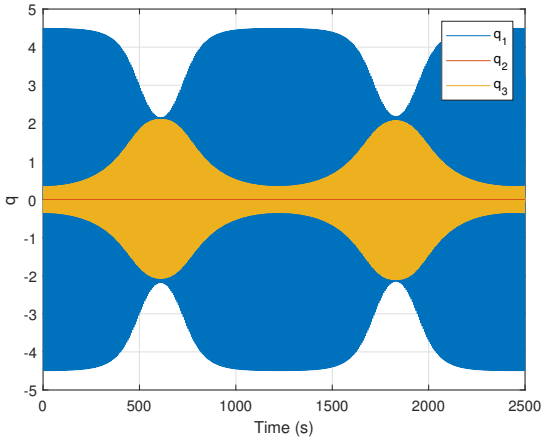

(d) $E = 9.7$

Figure 11: Time responses of the Hamiltonian system for several energy level in Fig. 9.

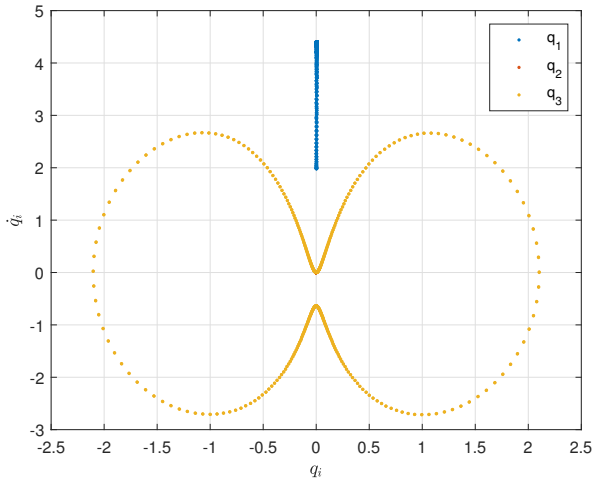

Figure 12: Poincaré section for the time response in Fig. 11d.

3.6.2. Neimark-Sacker bifurcation

In Fig. 8b, an unstable zone bounded by two Neimark-Sacker bifurcation points exists for mode 2. The co-existence of a stable quasi-periodic regime is therefore expected in this zone. In order to verify this assumption, numerical time integration is used to compute the response of the Hamiltonian system. This time integration is performed with the ode45 algorithm of Matlab with the following tolerances: RelTol $= 3 \times 10^{-14}$ and AbsTol $= 1 \times 10^{-15}$. For an initial energy $E = 10$, all the energy stays on the mode 2. This can be explain by the anti-symmetry of the mode 2 whereas the modes 1 and 3 are symmetric. However, for an initial energy $E = 50$, the numerical errors are amplified by the instability of the mode. Thus, the energy of the mode 2 is transferred to all other modes.

A Poincaré section is traced in Fig. 14 in order to estimate the nature of the behavior of the system. The periods are defined by the oscillations of the modal coordinate q_1 as previously. The behaviour seems to be not quasi-periodic. We evaluate the higher Lyapunov exponent in order to know if the response is chaotic. We compute the responses

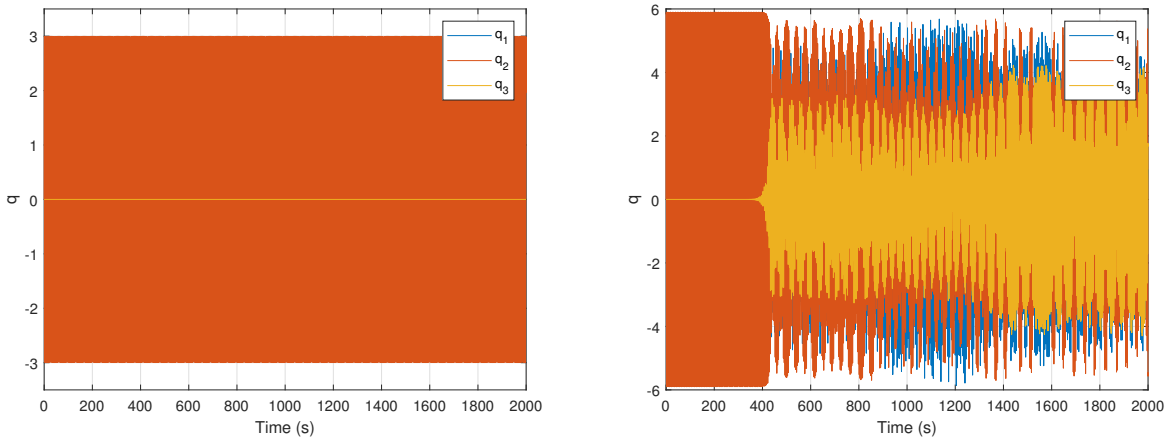

(a) $E = 10$ (b) $E = 50$

Figure 13: Response of the Hamiltonian system for several values of initial energy on mode 2.

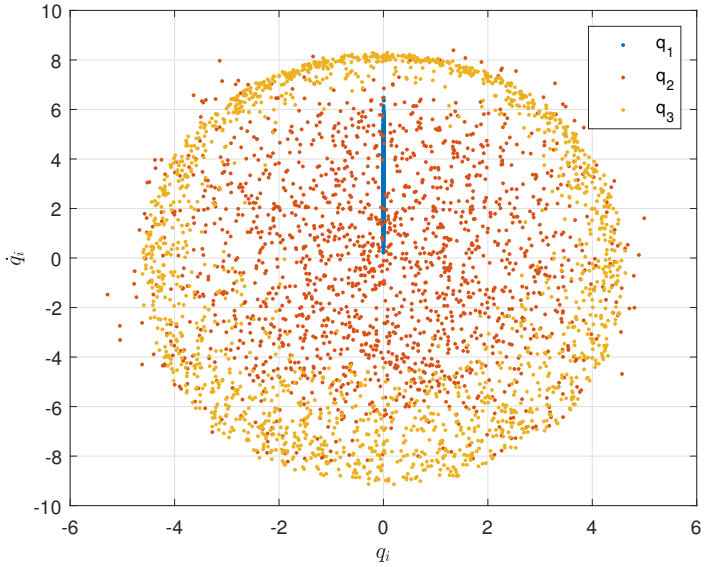

Figure 14: Section of Poincar between 2000 and 10 000 s of the Hamiltonian system for initial energy of 50 on mode 2.

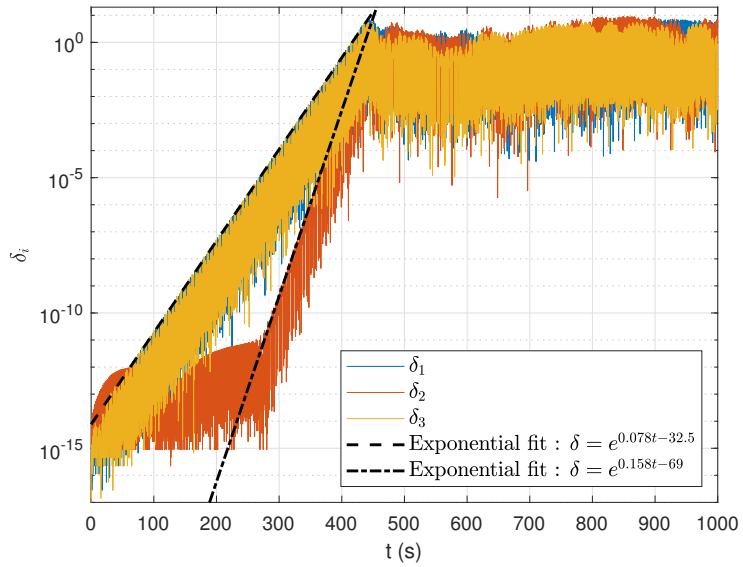

Figure 15: Difference between the modal coordinates of two responses with very close initial conditions.

of the system with two very close initial conditions [22, 23]: $E_1 = 50$ and $E_2 = 50 + 1 \times 10^{-14}$. The differences between each modal coordinates of the responses δ_i are traced in Fig. 15 in a semi logarithmic scale. The difference increases exponentially before to reach a plateau with the same order of magnitude as the response. This exponential growth shows a chaotic behaviour because for very close initial conditions the response can be completely different after some periods. The behaviour of the modal coordinate q_2 before $t = 280\,\mathrm{s}$ can be explained by the algorithm precision and rounding error of Matlab. The Lyapunov exponents can be evaluate with a fitting of the curves of the Fig. 15.

This time, the bifurcation does not allow energy to be transferred to a targeted mode. Instead, it is possible to distribute the energy from one mode to all the others. Thus, a Neimark-Sacker bifurcation can be used to define an energy threshold for which energy cannot be accumulated in the mode.

4. Increasing N

Now we increase N to see what kind of bifurcations are present in a longer chain and how they can generate exchanges of energy between non-linear modes. We consider a long non-linear chain of total mass M, total linear stiffness K and global damping coefficient C. The global internal and external non-linear coefficients are K_{int} and K_{ext}, respectively. To satisfy the global properties of the chain, the local coefficients are:

$$m = \frac{m_t}{N},\ c = \frac{c_t}{N},\ k = k_t N,\ k_{\mathrm{int}} = k_{t\mathrm{int}} N^3 \text{ and } k_{\mathrm{ext}} = \frac{k_{t\mathrm{ext}}}{N} \tag{31}$$

The frequency-energy plots are plotted for values of $N = 5, 10, 25$ in Fig. 16. We take the following values of parameters:

$$m_t = 1,\ c_t = 0,\ k_t = 1,\ k_{t\mathrm{int}} = 0,\ k_{t\mathrm{ext}} = 1 \tag{32}$$

We note that branch points and Neimark-Sacker bifurcations still exist. These bifurcations allow an exchange of energy between the different modes.

Moreover, with the exception of the first and last modes, the first Neimark-Sacker bifurcations of each mode seems to follow a smooth curve (represented with a dotted line in Fig. 16). On the last mode, a branch point appears before a Neimark-Sacker bifurcation.

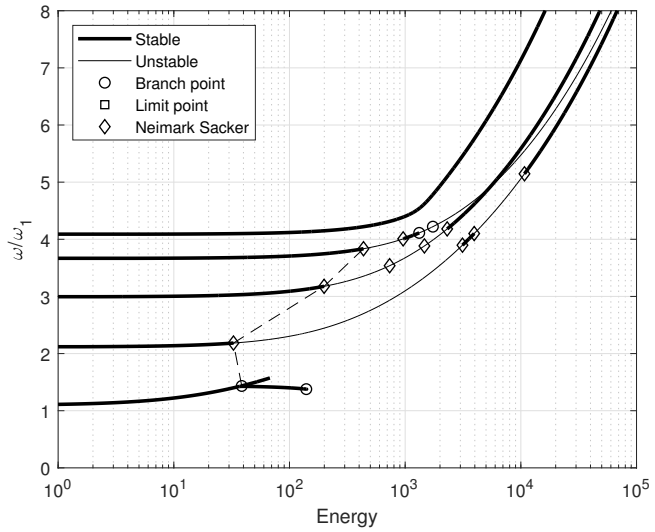

(a) N=5

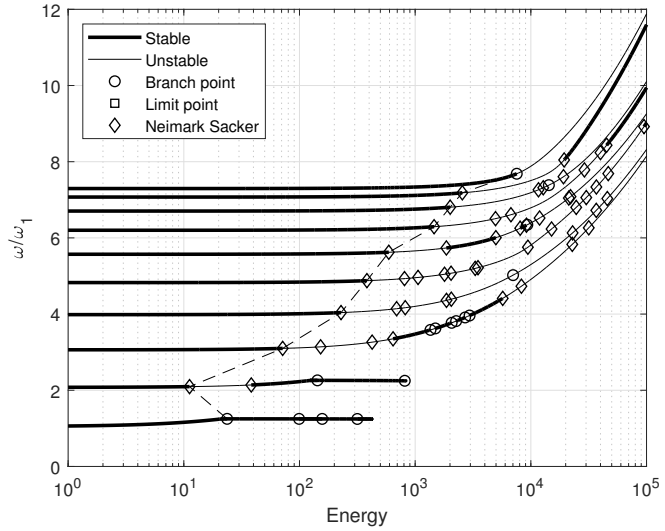

(b) N=10

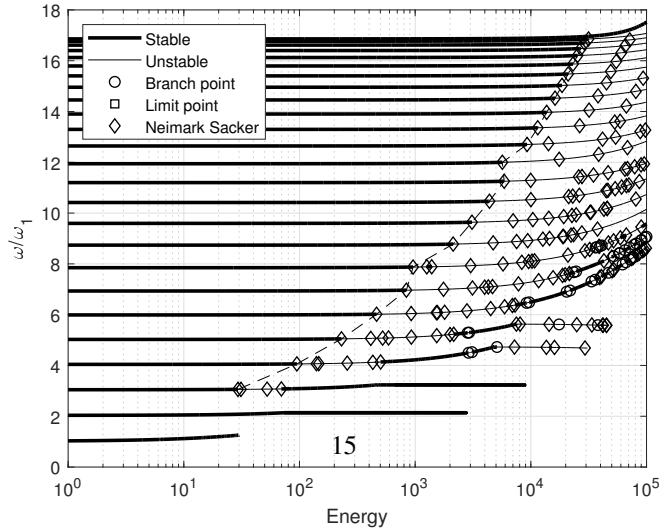

(c) N=25

Figure 16: Energy frequency diagrams of the system with non-linear modes and bifurcations for several values of N.

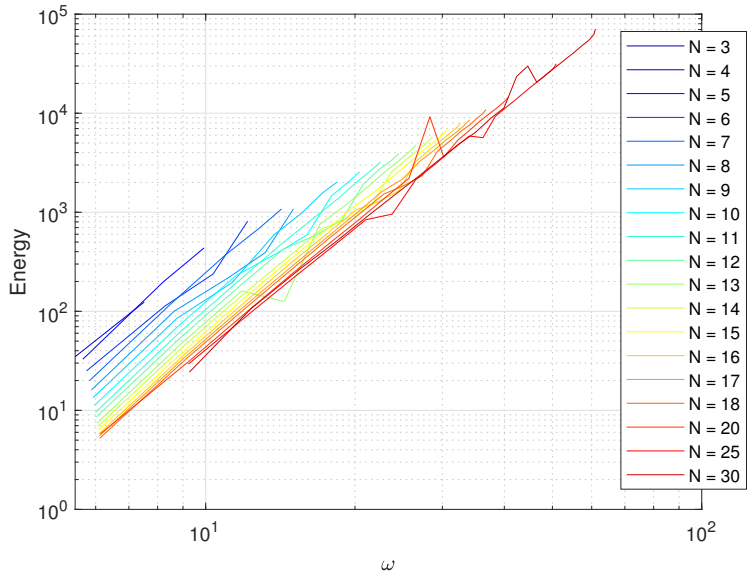

Figure 17: Energy of the first bifurcation of each mode for several values of N in logarithmic scales.

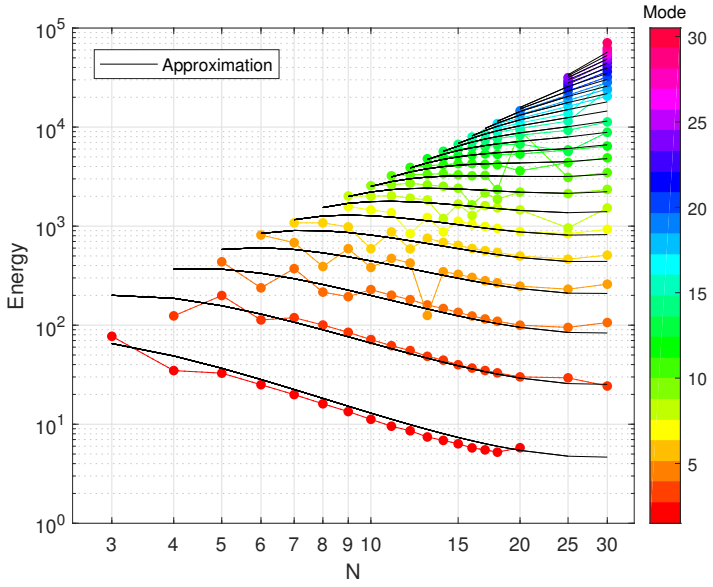

Figure 18: Energy of the first bifurcation of each mode for several values of N in logarithmic scale.

In Fig. 17, the energy of the first Neimark-Sacker bifurcation of each mode E_f is represented as a function of its frequency in a logarithmic scale for many values of N. We note that for each value of N the energy increases linearly in logarithmic scale.

From these curves, it is found that the energy of the first bifurcation can be approximated by the following energy-frequency relation:

$$E_f(\omega) = \alpha_N \omega^{\beta} \tag{33}$$

where α_N is a constant depending on the value of N and β a constant which can be evaluated by the least square method $\beta = 4.19$.

Then we plot in Fig. 18 the energy of the first bifurcation for each mode as a function of N in logarithmic scale. A new approximation is given as function of ω and N.

$$E_f(\omega, N) = \alpha N^{\gamma+N\delta}\omega^{\beta} \tag{34}$$

This approximation is plotted in Fig. 18 with the following coefficients:

$$\beta = 4.19,\ \gamma = 1.53,\ \delta = 0.02 \tag{35}$$

This distribution of the first Neimark-Sacker bifurcations is interesting. Indeed, in the previous section, we saw that these bifurcations correspond to an energy threshold beyond which the energy is distributed over all modes. Thus, this energy threshold can be given approximately as a function of N and the frequency of the mode. By playing with the parameters of the chain, it is possible to change the distribution of the energy thresholds.

5. Conclusion

We have proposed here to use the harmonic balance method to analyse a chain of oscillators with internal and external non-linearities. This method makes it possible to determine the non-linear modes and their stability. When considering a small system with only three masses, bifurcations can be identified: branching points lead to an energy exchange between two modes, while Neimark-Sacker bifurcations can lead to a chaotic behaviour. The latter results in an exchange of energy between all modes, but the manner of this exchange cannot be predicted. When considering a larger system with numerous degrees of freedom, a distribution of Neimark-Sacker bifurcations on the non-linear modes with increasing energy appears. This distribution can be used to define energy thresholds for which the energy of one mode will be dispersed over all the others.

Acknowledgements

This work was supported by the LABEX CeLyA (ANR-10-LABX-0060) of Universit de Lyon, within the program "Investissements dAvenir" operated by the French National Research Agency (ANR).

References

[1] L. I. Manevitch, A. Kovaleva, V. Smirnov, Y. Starosvetsky, Nonstationary Resonant Dynamics of Oscillatory Chains and Nanostructures, Springer Singapore, 2018. doi:10.1007/978-981-10-4666-7.

[2] A. Kovaleva, Response enhancement and energy localization in autoresonant nonlinear chains, International Journal of Non-Linear Mechanics 135 (2021) 103753. doi:10.1016/j.ijnonlinmec.2021.103753.

[3] A. F. Vakakis (Ed.), Normal Modes and Localization in Nonlinear Systems, Springer Netherlands, Dordrecht, 2001. doi:10.1007/978-94-017-2452-4.

[4] A. Kovaleva, Energy Transport and Localization in Weakly Dissipative Resonant Chains, in: I. Kovacic, S. Lenci (Eds.), IUTAM Symposium on Exploiting Nonlinear Dynamics for Engineering Systems, Vol. 37, Springer International Publishing, Cham, 2020, pp. 191–202, series Title: IUTAM Bookseries. doi:10.1007/978-3-030-23692-2_17.

[5] Y. A. Kosevich, L. I. Manevitch, A. V. Savin, Energy transfer in weakly coupled nonlinear oscillator chains: Transition from a wandering breather to nonlinear self-trapping, Journal of Sound and Vibration 322 (3) (2009) 524–531. doi:10.1016/j.jsv.2008.06.005.

[6] G. Iooss, G. James, Localized waves in nonlinear oscillator chains, Chaos: An Interdisciplinary Journal of Nonlinear Science 15 (1) (2005) 015113. doi:10.1063/1.1836151.

[7] Y. Starosvetsky, L. Manevitch, On intense energy exchange and localization in periodic FPU dimer chains, Physica D: Nonlinear Phenomena 264 (2013) 66–79. doi:10.1016/j.physd.2013.06.012.

[8] S. Charlemagne, C.-H. Lamarque, A. Ture Savadkoohi, Vibratory control of a linear system by addition of a chain of nonlinear oscillators, Acta Mechanica 228 (9) (2017) 3111–3133. doi:10.1007/s00707-017-1867-7.

[9] C.-H. Lamarque, A. T. Savadkoohi, S. Charlemagne, Experimental results on the vibratory energy exchanges between a linear system and a chain of nonlinear oscillators, Journal of Sound and Vibration 437 (2018) 97–109. doi:10.1016/j.jsv.2018.09.004.

[10] S. Flach, A. Ponno, The Fermi–Pasta–Ulam problem: Periodic orbits, normal forms and resonance overlap criteria, Physica D: Nonlinear Phenomena 237 (7) (2008) 908–917, publisher: Elsevier BV. doi:10.1016/j.physd.2007.11.017.

[11] F. Verhulst, High–low frequency interaction in alternating FPU α -chains, International Journal of Non-Linear Mechanics 131 (2021) 103686. doi:10.1016/j.ijnonlinmec.2021.103686.

[12] I. V. Andrianov, V. V. Danishevskyy, G. Rogerson, Supplementary material from "Vibrations of nonlinear elastic lattices: low- and high-frequency dynamic models, internal resonances and modes coupling", The Royal Society.doi:10.6084/M9.FIGSHARE.C.4915569.

[13] S. Charlemagne, A. Ture Savadkoohi, C.-H. Lamarque, Dynamics of a linear system coupled to a chain of light nonlinear oscillators analyzed through a continuous approximation, Physica D: Nonlinear Phenomena 374-375 (2018) 10–20. doi:10.1016/j.physd.2018.03.001.
[14] Y. A. Kuznetsov, Elements of Applied Bifurcation Theory, Vol. 112 of Applied Mathematical Sciences, Springer New York, New York, NY, 2004. doi:10.1007/978-1-4757-3978-7.
[15] T. Detroux, L. Renson, L. Masset, G. Kerschen, The harmonic balance method for bifurcation analysis of large-scale nonlinear mechanical systems, Computer Methods in Applied Mechanics and Engineering 296 (2015) 18–38. doi:10.1016/j.cma.2015.07.017.
[16] L. Xie, S. Baguet, B. Prabel, R. Dufour, Bifurcation tracking by Harmonic Balance Method for performance tuning of nonlinear dynamical systems, Mechanical Systems and Signal Processing 88 (2017) 445–461. doi:10.1016/j.ymssp.2016.09.037.
[17] R. Alcorta, S. Baguet, B. Prabel, P. Piteau, G. Jacquet-Richardet, Period doubling bifurcation analysis and isolated sub-harmonic resonances in an oscillator with asymmetric clearances, Nonlinear Dynamics 98 (4) (2019) 2939–2960. doi:10.1007/s11071-019-05245-6.
[18] B. Cochelin, C. Vergez, A high order purely frequency-based harmonic balance formulation for continuation of periodic solutions, Journal of Sound and Vibration 324 (1-2) (2009) 243–262. doi:10.1016/j.jsv.2009.01.054.
[19] L. Peletan, S. Baguet, M. Torkhani, G. Jacquet-Richardet, A comparison of stability computational methods for periodic solution of nonlinear problems with application to rotordynamics, Nonlinear Dynamics 72 (3) (2013) 671–682. doi:10.1007/s11071-012-0744-0.
[20] M. Peeters, R. Viguié, G. Sérandour, G. Kerschen, J.-C. Golinval, Nonlinear normal modes, Part II: Toward a practical computation using numerical continuation techniques, Mechanical Systems and Signal Processing 23 (1) (2009) 195–216. doi:10.1016/j.ymssp.2008.04.003.
[21] M. Volvert, G. Kerschen, Phase resonance nonlinear modes of mechanical systems, Journal of Sound and Vibration 511 (2021) 116355. doi:10.1016/j.jsv.2021.116355.
[22] A. Wolf, J. B. Swift, H. L. Swinney, J. A. Vastano, Determining Lyapunov exponents from a time series, Physica D: Nonlinear Phenomena 16 (3) (1985) 285–317. doi:10.1016/0167-2789(85)90011-9.
[23] S. H. Strogatz, Nonlinear dynamics and chaos: with applications to physics, biology, chemistry, and engineering, second edition Edition, Westview Press, 2015.